The Astrophysical Journal, 628:76–88, 2005 July 20
© 2005. The American Astronomical Society. All rights reserved. Printed in U.S.A.

A THEORETICAL STUDY OF THE LUMINOSITY-TEMPERATURE RELATION FOR CLUSTERS OF GALAXIES

A. Del Popolo,[1] N. Hiotelis,[2] and J. Peñarrubia[3]
Received 2004 October 18; accepted 2005 February 21

ABSTRACT

A luminosity-temperature relation is derived for clusters of galaxies. The two models used take into account the angular momentum acquisition by the protostructures during their expansion and collapse. The first model is a modification of the self-similar model, while the second is a modification of the punctuated equilibria model of Cavaliere et al. In both models the mass-temperature relation (*M-T*) used is based on previous calculations of Del Popolo. We show that the above models lead, in X-rays, to a luminosity-temperature relation that scales as $L \propto T^5$ at the scale of groups, flattening to $L \propto T^3$ for rich clusters and converging to $L \propto T^2$ at higher temperatures. However, a fundamental result of our paper is that the nonsimilarity in the *L-T* relation can be explained by a simple model that takes into account the amount of angular momentum of a protostructure. This result is in disagreement with the widely accepted idea that the nonsimilarity is due to nongravitating processes, such as heating and/or cooling.

Subject headings: cosmology: theory — galaxies: formation — large-scale structure of universe

1. INTRODUCTION

Observations of clusters of galaxies (e.g., *ROSAT*, *ASCA*) performed in the past decade have shown the existence of a tight correlation between the total gravitating mass of clusters ($M_{\rm tot}$), their X-ray luminosity ($L_{\rm X}$), and the temperature ($T_{\rm X}$) of the intracluster medium (ICM) (David et al. 1993; Markevitch 1998; Horner et al. 1999). The importance of these relations is due to the fact that cluster masses are difficult to measure directly, and when comparing cluster observations with models of structure formation, a surrogate for cluster mass is used. Since $M_{\rm tot}$ compares with the ICM temperature measurements that can be obtained through X-ray spectroscopy, the *M-T* relation is important. On one hand, the X-ray temperature measures the depth of the potential wells, and the bolometric luminosity, $L \propto n^2 R_{\rm X}^3 T^{1/2}$, emitted as thermal bremsstrahlung by intracluster plasma measures the baryon number density n within the volume $R_{\rm X}^3$. Until some years ago, the cluster structure was considered to be scale-free, which means that the global properties of clusters, such as halo mass, luminosity-temperature, and X-ray luminosity would scale self-similarly (Kaiser 1986). In particular, the gas temperature would scale with cluster mass as $T \propto M^{2/3}$ and the bolometric X-ray luminosity would scale with temperature as $L \propto T^2$, in the bremsstrahlung-dominated regime above $\sim$2 keV.[4]

Studies following that of Kaiser (1986) showed that the observed luminosity-temperature relation is closer to $L \propto T^3$ (e.g., Edge & Stewart 1991), indicating that nongravitational processes should influence the density structure of a cluster's core, where most of the luminosity is generated (Kaiser 1991; Evrard & Henry 1991; Navarro et al. 1995; Bryan & Norman 1998). One way to obtain a scaling law closer to the observational one is to have nongravitational energy injected into the ICM before or during cluster formation. This solution, called preheating, was originally invoked to solve two related problems: (1) to explain (Kaiser 1991; Evrard & Henry 1991)[5] the apparent negative evolution of the X-ray cluster luminosity function (Gioia et al. 1990; Henry et al. 1992) from the *Einstein* Medium Sensitivity Survey in a $\Omega_m = 1$ universe, and (2) to explain (White 1991)[6] why groups and low-mass clusters seem to have higher X-ray temperatures than expected based on member velocity dispersions.

The mechanisms proposed to explain the slope change of the *L-T* relation can be divided into three main categories:

1. Models that include a preheating of the gas within a cluster. Ponman et al. (1999) showed that the entropy of the ICM in the center of low-temperature clusters is greater than the value expected from gravitational collapse. It has been shown that models that include an additional gas entropy can successfully reproduce many observational properties (Bower et al. 1997; Cavaliere et al. 1997, 1999; Tozzi & Norman 2001; Borgani et al. 2001; Voit & Brian 2001).

2. Models that implement feedback processes that alter the gas characteristics during the evolution of the cluster. In principle, there are many different physical processes that could break the self-similar scaling, including heating from supernovae or active galactic nuclei, or the removal of low-entropy gas via radiative cooling with subsequent supernova heating (Voit & Bryan 2001). Another example is that of Muanwong et al. (2001), who simulated galaxy cluster formation including radiative cooling with cool gas dropout and was able to reproduce the $L \propto T^3$ dependence, without adding any entropy to the gas. Moreover, other possibilities such as magnetic pressure or cosmic-ray pressure have not been ruled out. Allen & Fabian (1998) have examined the effects of cooling flows for a sample of the most X-ray–luminous clusters ($L_{\rm bol} > 10^{45}$ ergs s^{-1}), finding a flattening from $L \propto T^3$ to $L \propto T^2$, in agreement with

[1] Physics Department, Boğaziçi University, 80815 Bebek, Istanbul, Turkey.
[2] First Experimental Lyceum of Athens, Ipitou 15, Plaka 10557, Athens, Greece.
[3] Max-Planck-Institut für Astronomie, Königsstuhl 17, 69117 Heidelberg, Germany.

[4] Indeed, numerical simulations that include gas dynamics but exclude nongravitational processes such as radiative cooling and supernova heating produce clusters that obey these scaling laws (e.g., Evrard et al. 1996; Bryan & Norman 1998; Thomas et al. 2002).

[5] Kaiser's self-similar model predicts $L \propto T^{3.5}$. Evrard & Henry (1991) obtained the relation $L \propto T^{11/4}$.

[6] In this case preheating was in the form of supernova-driven galactic winds.

models that include the effects of shocks and preheating on the X-ray gas (Cavaliere et al. 1997, 1999). Cavaliere et al. (1997, 1998) have constructed a model in which the observed *L-M* relation on both cluster and group scales can be reproduced by varying the gas density at the virial radius, according to the accretion-shock strength, as determined by the temperature difference between the infalling and virialized gases. Another possibility to explain the *L-T* relation are systematic variations in the baryonic fraction with cluster mass (David et al. 1993). To distinguish among these processes, observations of high-redshift groups and clusters will be crucial to measure the evolution of the observed scaling relations as a function of redshift.

3. Hydrodynamic models that do not include gas preheating or feedback processes, which also reproduce the available observational data (e.g., Bryan & Norman 1998). Throughout this paper, we will analyze this last scenario.

On the other hand, the mass-temperature relation seemed like it ought to be more fundamental and less sensitive to nongravitational effects. Yet, observations collected over the last few years indicate that this relation also disagrees with both the scale-free predictions and simulations that exclude nongravitational processes (Horner et al. 1999; Nevalainen et al. 2000; Finoguenov et al. 2001; Xu et al. 2001). These results derive mostly from resolved X-ray and temperature profiles coupled with the assumption of hydrostatic equilibrium, and they do seem consistent with gravitational lensing measurements (Allen et al. 2001). Understanding the scaling properties of clusters is of broad importance because these scaling laws are integral to determination of cosmological parameters. Thus, any inaccuracies in the mass-temperature relation propagate into uncertainties in cosmological parameters derived from clusters (e.g., Voit 2000, hereafter V00).

In Del Popolo (2002b), we derived the mass-temperature relation and its time evolution for clusters of galaxies in different cosmologies. We use two different models: the first one is a modification and improvement of a model by Del Popolo & Gambera (1999) based on a modification of the top-hat model in order to account for angular momentum acquisition by protostructures and for an external pressure term in the virial theorem. The second one is an improvement of a model proposed by V00, again to account for the angular momentum acquired by protostructures during their formation. Both models showed that the *M-T* relation is not self-similar. A break is present in the quoted relation at $T \sim 3$ keV and, at the lower mass end, the power-law index of the *M-T* relation is larger than $\alpha = 3/2$ even in flat universes. The slope of the power-law index depends on the considered cosmology. The two models also agree in predicting a more modest time evolution (which also depends on the cosmology) of the quoted relation in comparison with the results of previous models.

This is in agreement with studies showing that the self-similarity in the *M-T* relation seems to break at a few keV (Nevalainen et al. 2000; Xu et al. 2001). By means of *ASCA* data for a small sample of nine clusters (six at 4 keV and three at $\sim$1 keV), Nevalainen et al. (2000) have shown that $M_{\rm tot} \propto T_{\rm X}^{1.79\pm0.14}$ for the whole sample, and $M_{\rm tot} \propto T_{\rm X}^{3/2}$ excluding the low-temperature clusters. Xu et al. (2001) have found $M_{\rm tot} \propto T_{\rm X}^{1.60\pm0.04}$ using the β-model, and $M_{\rm tot} \propto T_{\rm X}^{1.81\pm0.14}$ by means of the Navarro et al. (1995) profile. Finoguenov et al. (2001) have investigated the *T-M* relation in the low-mass end, finding that $M \propto T^{\sim 2}$, and $M \propto T^{\sim 3/2}$ at the high-mass end. This behavior has been attributed to the effect of the formation redshift (Finoguenov et al. 2001; but see Mathiesen 2001 for a different point of view), or to cooling processes (Muanwong et al. 2001) and heating (Bialek et al. 2001). Afshordi & Cen (2002, hereafter AC02) have shown that nonsphericity introduces an asymmetric, mass-dependent scatter for the *M-T* relation, altering its slope at the low-mass end ($T \sim 3$ keV).

The *L-T* and *M-T* relations are somehow related: as shown by Shimizu et al. (2003), it is possible to make a reliable prediction for the *L-T* relation once the *M-T* relation is specified. In turn, one can obtain the *M-T* relation that reproduces the observed *L-T* relation without assuming an ad hoc model for the thermal evolution of intracluster gas. The two relations (*M-T* and *L-T*) are strictly connected.

This conclusion in turn indicates that the *L-T* relation provides a good diagnosis of the underlying *M-T* relation, which is as yet poorly determined observationally.

Apart from the physical mechanism of the additional thermal processes, there are three effects that might modify the mass dependence of X-ray luminosity and steepen the resulting *L-T* relation. First, the gas density profile might be significantly flatter for less massive systems. Second, the mass dependence of the hot-gas mass fraction is strong as $f_{\rm gas} \propto M_{\rm vir}^{1/3}$. Finally, the mass-temperature relation is $T_{\rm gas} \propto M_{\rm vir}^{2/5}$. In practice, a realistic model should be a combination of these three effects to some extent.

In this paper we derive a luminosity-temperature relation for clusters of galaxies that takes into account the amount of the angular momentum of protostructures. We use two different models: the first (which we call MSSM) is a modification of the self-similar model (SSM), while the second one is a modification of the punctuated equilibria model (MPEM) (Cavaliere et al. 1999). We show that the presence of the angular momentum during the gravitational collapse leads to a non–self-similar *L-T* relation. The two models used are described in § 2. The results are presented and discussed in § 3, and the conclusions are summarized in § 4.

2. MODEL

2.1. *Modified Self-Similar Model for the L-T Relation*

The *L-T* relation constitutes a fundamental link between the physics of the baryon component and the dynamical properties of the dark matter (DM) condensations. The simplest model describing that relation is the SSM model (Kaiser 1986), obtained assuming that the gas density or the baryon number density n is proportional to the average DM density ρ and that the virial radius $R_{\rm vir}$ is proportional to $R_{\rm X}$ (see § 1 for a definition). In this way, one obtains, according to this last, $L \propto M_{\rm vir}\rho T^{1/2}$. In fact, $T \propto M_{\rm vir}/R_{\rm vir}$, $n \propto \rho \propto M_{\rm vir}/R_{\rm vir}^3$, $R_{\rm vir} \propto R_{\rm X}$, and $L \propto \int_0^{R_{\rm vir}} \rho^2 T^{1/2} r^2 dr \propto \rho^2 T^{1/2} R_{\rm vir}^3$, and recalling that $R_{\rm vir} \propto (M_{\rm vir}/\rho)^{1/3}$ leads to $L \propto \rho M_{\rm vir} T^{1/2}$ or recalling that $R_{\rm vir} \propto (T/\rho)^{1/3}$, we get $L \propto \rho^{1/2} T^2$. This last result is inconsistent with observed correlation close to $L \propto T^3$ (Edge & Stewart 1991; Mushotzky 1994). In addition, a further steepening at the temperature of galaxy groups is indicated for thermal emission not associated with single galaxies (Ponman et al. 1999).

In the following, we derive a modified SSM, showing that slope of the *L-T* relation changes at different scales.

Using the notation of Balogh et al. (1999), let us begin with a cluster with gas temperature $T(r)$ and density profile $\rho(r)_g$ for which the bolometric X-ray luminosity from bremsstrahlung scales as

$$L = \frac{6\pi k}{C_1(\mu m_p)^2} \int_0^{R_{\rm vir}} r^2 \rho_g(r)^2 T_g(r)^{1/2} dr \qquad (1)$$

(see Balogh et al. 1999), where $C_1 = 3.88 \times 10^{11}$ s K$^{-1/2}$ cm^{-3}, $\mu = 0.59$, and $R_{\rm vir} \propto (M_{\rm vir}/\rho)^{1/3}$ is the virial radius, where $\rho(z) \propto (1+z)^3$ is the DM density in the cluster, proportional to the average cosmic DM density ρ_u at formation. The simplest model describing the *L-T* relation, which can be calculated by equation (1), is the SSM (Kaiser 1986), assuming that $\rho_g \propto \rho$.

We only consider halos in which not all of the gas within $R_{\rm vir}$ has had time to cool since the halo formed.

We assume a singular, truncated isothermal sphere for the DM potential, $\rho(r) = \rho_R (r/R_{\rm vir})^{-2}$, where ρ_R is the density at the virial radius $R_{\rm vir}$ and is equal to a third of the mean density *within* $R_{\rm vir}$, $\bar{\rho}(R_{\rm vir})$. This latter quantity is related to the critical density at redshift z by $\bar{\rho}(R_{\rm vir}) = \Delta_c(z)\rho_c(z)$, and $\Delta_c = 78\Omega(z) + 80 + 300\Omega(z)/[1+15\Omega(z)]$ is a fit, accurate to better than 2%, to the results of the spherical collapse model as presented in Eke et al. (1996). It will be convenient to define a redshift evolution term, $F_1(z)^2 = (1+z)^2(1+\Omega_0 z)\Delta_c(z)/\Delta_c(0)$, so that

$$\rho_R = \frac{1}{3}\Delta_c(0)\rho_c(0)F_1(z)^2. \tag{2}$$

For $\Omega_0 = 1$, $F_1(z)^2 = (1+z)^3$ and $\Delta_c = 178$. In this model, we make the common assumption (e.g., Eke et al. 1996) that the gas is distributed isothermally, with a temperature equal to the virial temperature of the halo. If the gas is dissipationless, its density profile will match that of the DM, i.e.,

$$\rho_g(r) = \rho_{g,R}(r/R_{\rm vir})^{-2}, \tag{3}$$

and $\rho_{g,R}/\rho_R = \Omega_b/\Omega_0$. To avoid the singularity at $r = 0$ when integrating over the assumed isothermal profile, an arbitrary core radius of $r_c = f_c R_{\rm vir}$ is adopted with $f_c = 0.1$, such that $\rho_g(r < r_c) = \rho_g(r_c)$. The integral in equation (1) is dominated by the contribution from within a few core radii, and thus the scaling properties of this integral depend weakly on the assumed density profile. Furthermore, departures from the standard profile can be accommodated by redefining the core radius of the system.

In order to obtain the luminosity-mass relation, we evaluate equation (1) and use the *M-T* relation, which takes into account the angular momentum of the protostructure, which is obtained in Appendix C:

$$kT \simeq 8\ {\rm keV}\left(\frac{M^{2/3}}{10^{15}\ h^{-1}\ M_\odot}\right)\left[\frac{1}{m_1} + \left(\frac{t_\Omega}{t}\right)^{2/3} + \frac{K_1(m_1,x)}{M^{8/3}}\right] \times \left[\frac{1}{m_1} + \left(\frac{t_\Omega}{t_0}\right)^{2/3} + \frac{K_0(m_1,x)}{M_0^{8/3}}\right]^{-1}, \tag{4}$$

where $K_1(m_1,x)$ is given by[7]

$$K_1(m_1,x) = (m_1-1)Fx\,{\rm LerchPhi}\left(x,\ 1,\ \frac{3m_1}{5+1}\right) - (m_1-1)F\,{\rm LerchPhi}\left(x,\ 1,\ \frac{3m_1}{5}\right), \tag{5}$$

where

$$F = \frac{2^{7/3}\pi^{2/3}\xi\rho_b^{2/3}}{3^{2/3}H^2\Omega}\int_0^r \frac{\mathcal{L}^2 dr}{r^3}, \tag{6}$$

[7] $K_0(m_1,x)$ indicates that $K_1(m_1,x)$ must be calculated assuming $t = t_0$.

$m_1 = 5/(n+3)$, $t_\Omega = \pi\Omega_0/H_0(1-\Omega_0-\Omega_\Lambda)^{3/2}$, $x = 1+(t_\Omega/t)^{2/3}$, which is connected to mass by $M = M_0 x^{-3m_1/5}$ (V00), and $\xi = r_{\rm ta}/x_1$, where $r_{\rm ta}$ is the turnaround radius and x_1 is defined by the relation $M = 4\pi\rho_b x_1^3/3$, where ρ_b is the background density. Finally, we get

$$L = 3.31\times 10^{45}\left(\frac{M}{M_0}\right)^{4/3}\left(\frac{1}{178}\Delta_c\right)F_1^2\left(\frac{\Omega_b}{\Omega}\right)^2 \times \sqrt{\frac{1/m_1 + (t_\Omega/t)^{2/3} + K_1(m_1,x)/(M/M_0)^{8/3}}{1/m_1 + (t_\Omega/t)^{2/3} + K_0(m_1,x)/M_0^{8/3}}}\left(\frac{1-fc}{fc}\right), \tag{7}$$

which, differently from Kaiser's (1986) prediction, is not self-similar. It reduces to the self-similar form ($L \propto M^{4/3}$) if angular momentum acquisition is not taken into account, namely, if $\mathcal{L} \to 0$ (or $F \to 0$).

The previous computation depends on the value of the angular momentum acquired by the DM halos from tidal torques from surrounding matter. This enters the *L-T* relation through the quantities F and K_1 (see also Appendix A). In the limit of vanishing angular momentum, the *L-T* and *M-T* relations reduce to the well-known self-similar forms. Thus, it is important to add a discussion on the magnitude of the angular momentum calculated as in previous papers (e.g., Del Popolo & Gambera 1998; Del Popolo et al. 2001).

The angular momentum is acquired by the cosmological torque acting on the protostructures due to the tidal field of the environment. The amount of angular momentum as well as its distribution are related to the assumed power spectrum of density perturbations. We have to note here that the problem of the growth of angular momentum of protostructures from the tidal torques of the surrounding matter has been studied extensively in the literature with both analytical and numerical (*N*-body) methods (e.g., Efstathiou & Jones 1979; Barnes & Efstathiou 1987; Voglis & Hiotelis 1989; Warren et al. 1992; Eisenstein & Loeb 1995; Kratsov et al. 1998). A main result of the above studies is that the values of the dimensionless spin parameter $\lambda \equiv \mathcal{L}|E|^{1/2}/GM^{5/2}$ (Peebles 1971) follow a lognormal distribution with a small average value of 0.05. In the above relation, $\mathcal{L}$ is the total angular momentum of the protostructure, E is its binding energy, M is its mass, and G is the gravitational constant. The above numerical results are confirmed by analytical studies presented by other authors, such as those of Steinmetz & Bartelmann (1995) and Catelan & Theuns (1996). To be more precise, λ depends on the galactic morphological type, being as high as $\lambda \simeq 0.5$ for spirals and SO galaxies and $\lambda \simeq 0.05$ for ellipticals, although the dispersion around these values is large (Efstathiou & Jones 1979). In the case of structures of 10^{12}–$10^{13}\ M_\odot$ its value is $\simeq$0.1, and $\simeq$0.01 for clusters.[8]

In this paper, we calculate angular momentum as in § 3 of Del Popolo et al. (2001), following Eisenstein & Loeb (1995). With the Bardeen et al. (1986) power spectrum smoothed on galactic scale for a $\nu = 2$ peak, the model gives a value of 2.5×10^{74} g cm^2 s^{-1}, in very good agreement with Catelan & Theuns (1996); in other words the amount of angular momentum used in our calculations is consistent with the values of λ predicted by the tidal fields of the surrounding matter. Although this amount is in general small, our results show that it is efficient to lead to a nonsimilar

[8] The resulting typical circular velocities of structures is $\simeq$150 km s^{-1} for galaxies similar to the Milky Way, $\simeq$5 km s^{-1} for clusters, and $\simeq$10 km s^{-1} for superclusters (see Catelan & Theuns 1996).

L-T relation. The angular momentum of DM halos also has other important consequences. For example, small amounts of angular momentum are able to change the density profile of DM halos from the isothermal law $\rho(r) \propto r^{-2}$ to a profile that flattens significantly inward (e.g., Hiotelis 2002).

Moreover, several studies have shown that the influence and the role of shear on structure formation is of fundamental importance. Shear on a density perturbation can be produced by the intrinsic asphericity of the perturbation itself (internal shear), or it can be due to the interaction of the perturbation with the neighboring ones (external shear). For example, according to the previrialization conjecture (Peebles & Groth 1976; Davis & Peebles 1977; Peebles 1990), initial asphericities and tidal interactions between neighboring density fluctuations induce significant nonradial motions that oppose the collapse. This means that virialized clumps form later, with respect to the predictions of the linear perturbation theory or the spherical collapse model, and that the initial density contrast needed to obtain a given final density contrast must be larger than that for an isolated spherical fluctuation. This kind of conclusion was supported by Barrow & Silk (1981), Szalay & Silk (1983), Villumsen & Davis (1986), Bond & Myers (1993a, 1993b), and Lokas et al. (1996). Arguments based on a numerical least-action method led Peebles (1990) to the conclusion that irregularities in the mass distribution, together with external tides, induce nonradial motions that slow down the collapse. In a more recent paper, Audit et al. (1997) conclude that spherical collapse is the fastest. This result is in agreement with Peebles (1990) and more recent papers, namely, Del Popolo et al. (2001) and Del Popolo (2002a).

2.2. *Improvements to the Punctuated Equilibria Model*

In this subsection, we extend the punctuated equilibria model (PEM) by Cavaliere et al. (1997, 1998, 1999; hereafter CMT97, CMT98, CMT99) to take account of angular momentum acquisition from the protostructure. In their model (CMT98), the cluster evolution is described as a sequence of "punctuated equilibria," that is to say, a sequence of hierarchical merging episodes of the DM halos, associated in the intracluster plasma (ICP) with shocks of various strengths (depending on the mass ratio of the merging clumps), which provide the boundary conditions for the ICP to readjust to a new hydrostatic equilibrium.

The X-ray bolometric luminosity of a cluster is given by equation (1), which in CMT98's notation is

$$L \propto \int_0^{r_2} n^2(r) T^{1/2}(r)\, d^3 r. \tag{8}$$

Here $T(r)$ is temperature in the plasma and r_2 is the cluster boundary, which we take to be close to the virial radius $R_{\rm vir} \propto M_{\rm vir}^{1/3} \rho^{-1/3}$, where $\rho(z) \propto (1+z)^3$ is the DM density in the cluster, proportional to the average cosmic DM density $\rho_u(z)$ at formation.

As shown in Appendix B, the L-T relation can be cast in the form

$$L \propto \left(\frac{n_2}{n_1}\right)^2 \rho \left(\frac{T_2}{T_v}\right)^{1/2} \overline{\left[n(r)/n_2\right]^{2+(\gamma-1)/2}}\, m^{4/3} \times \sqrt{\frac{1/m_1 + (t_\Omega/t)^{2/3} + K_1/(m/m_0)^{8/3}}{1/m_1 + (t_\Omega/t)^{2/3} + K_0/m_0^{8/3}}}. \tag{9}$$

See Appendix B for a derivation of equation (9) and a definition of the terms involved.

Our final aim is to compute the average value of L and its dispersion, associated with a given cluster mass m. In order to reach this goal, we must sum over the shocks produced at a time $t' < t$ in all possible progenitors m' (weighting with their number) by the accreted clumps Δm (weighting with their merging rate); finally, we integrate over times t' from an effective lower limit $t - \Delta t$.

The average L is then given by

$$\langle L \rangle = Q \int_{t-\Delta t}^{t} dt' \int_0^m dm' \int_0^{m-m'} d\Delta m \frac{df}{dm'}(m', t'|m, t) \times \frac{d^2 p(m' \to m' + \Delta m)}{d\Delta m\, dt'} L, \tag{10}$$

and the variance is given by

$$\langle \Delta L^2 \rangle = Q \int_{t-\Delta t}^{t} dt' \int_0^m dm' \int_0^{m-m'} d\Delta m \frac{df}{dm'}(m', t'|m, t) \times \frac{d^2 p(m' \to m' + \Delta m)}{d\Delta m\, dt'} (L - \langle L \rangle)^2, \tag{11}$$

where Q is the normalization factor (the compounded probability distribution in eqs. [10] and [11] has been normalized to 1). The effective lower limit for the integration over masses is set as described in § 2.4 of CMT99.

3. RESULTS

The results of our calculation are plotted in Figures 1–3. In Figure 1 we plot a direct comparison between the SSM (*long-dashed line*), MSSM (*short-dashed line*), PEM[9] (*solid line*), and finally MPEM with a tilted CDM cosmogony (*dotted line*). As is well known, the SSM predicts that $L \propto T^2$ (Kaiser 1986), while the MSSM predicts non–self-similar behavior of the L-T relation, namely, an L-T relation $L \propto T^5$ on the scale of groups and $L \propto T^3$ for rich clusters, in agreement with observations, and the L-T relation saturates toward $L \propto T^2$ for higher temperatures. The plot shows that the MSSM predicts a behavior of the L-T relation similar to that predicted by the PEM. Differences of a maximum of 10% are noted for smaller values of the temperature.

We note above that a self-similar evolution for all clusters at typical cluster temperatures ($T > 2$ keV) should lead to $L \propto T^2$, since free-free emission dominates the cooling. Instead, the observed L-T relation is more steep, $L \propto T^{2.6-2.9}$, meaning that lower temperature clusters and groups of galaxies are far less luminous than expected. Several different models have been proposed in order to explain the quoted behavior in the L-T relation. The key point of these models is that the X-ray luminosities of low-temperature clusters are small because their gas is less centrally concentrated than in hotter clusters, an effect that has been attributed to a universal minimum entropy level in

[9] The PEM is based on hierarchical clustering. Group and cluster formation is envisaged in terms of DM potential wells evolving hierarchically and engulfing outer baryons by accretion of smooth gas or by merging with other clumps. After a merging episode, the ICP in the wells falls back to a new, approximate hydrostatic equilibrium. This sequence of hydrostatic equilibria of the ICP is physically motivated for all merging events except for those involving comparable clumps (a mass ratio larger than ~1/4). However, these sum up to less than 10% in the number. In the PEM, thermal energy of the infalling gas is initially due to stellar preheating (of nuclear origin); then it is increased to the virial value (of gravitational origin) when the accreted gas is bound in DM subclumps. So the preheating sets an effective threshold $kT_1 \sim 0.5$ keV to gas inclusion, which breaks the self-similar correlation $L \propto T^2$ not only in its vicinity but also up to a few keV.

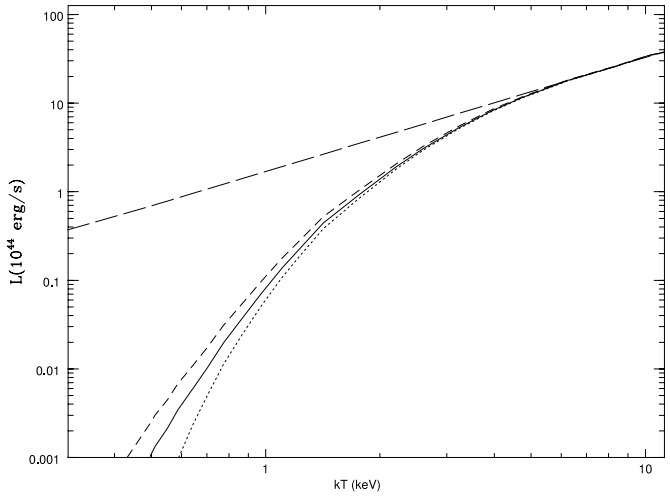

FIG. 1.—Comparison between the SSM (*long-dashed line*), MSSM (*short-dashed line*), PEM (*solid line*), and MPEM (*dotted line*).

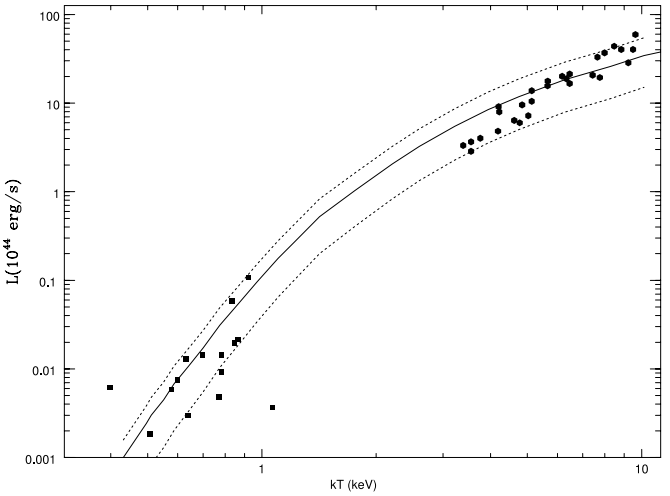

FIG. 3.—Similar to Fig. 2, but for the MSSM model.

intracluster gas resulting from supernova heating (Ponman et al. 1999; Wu et al. 2000; CMT99), from heating by active nuclei (Wu et al. 2000), or from radiative cooling (Wu et al. 2000; Bryan 2000). In other terms, for some reasons the core gas is less high than that expected in the self-similar model. For example, an early episode of uniformly distributed supernova feedback could rectify the problem by heating the uncondensed gas and therefore making it harder to compress in the core. In other words, the models with preheating and similar processes give rise to the quoted break because they change the density in the core. During the hierarchical buildup an energy input preheats the gas before it falls into new groups and clusters, thus hindering its flow into the latter. The core density decreases, and thus so does the luminosity.

A similar mechanism acts in the model of this paper. In fact, as shown in Del Popolo & Gambera (1998), the angular momentum acquired by a shell centered on a peak in the CDM density distribution is anticorrelated with density: high-density peaks acquire less angular momentum than low-density peaks (Hoffman 1986; Ryden 1988). A greater amount of angular momentum acquired by low-density peaks (with respect to the high-density ones) implies that these peaks can more easily resist gravitational collapse, that consequently it is more difficult for them to form structure, and that in some conditions the structure formation by low-mass peaks is even inhibited.[10]

The break of the self-similarity of the *L-T* relation may also have important consequences for determining the cluster masses from their luminosity. As shown by Shimizu et al. (2003), the predicted *L-T* relation is very sensitive to the assumed *M-T* relation, and thus the non–self-similarity of the *L-T* relation is strictly connected to that in the *M-T* relation. The *M-T* relation, as previously discussed, is also non–self-similar, and this behavior has been interpreted in different ways (see § 1). In Del Popolo (2002b), the bend in the *M-T* relation is entirely justified in terms of tidal interaction among neighboring clusters, or in other terms, it is strictly connected to the asphericity of clusters (see Del Popolo & Gambera 1999 for a discussion on the relation between angular momentum acquisition, asphericity, and structure formation). Nonsphericity introduces an asymmetric bend, dependent on mass, in the *M-T* relation that gives rise to a different slope at the low-mass end ($T \sim 3$ keV): the lower the mass, the larger the bend.

This result is in agreement with AC02's result. In that paper, the authors used a nearly spherical collapsing region to obtain the *M-T* relation. According to their results, nonsphericity introduces an asymmetric, mass-dependent scatter (the lower the mass, the larger the scatter) for the *M-T* relation, thus altering the slope at the low-mass end ($T \simeq 3$ keV).

As noted in § 1, heating/cooling mechanisms are not necessary to explain the observational *L-T* correlation. Bryan & Norman (1998), carrying out large hydrodynamic simulations that followed the hierarchical evolution of clusters of galaxies, found that the observed *M-T*, *L-T* relations can be thoroughly reproduced if the number of particles and the spatial resolution are large enough. The importance of the numerical accuracy proves to be crucial to determining those relations, and so, for example, Muanwong et al. (2001), using simulations with only 160^3 particles and a spatial resolution of 100 h^{-1} Mpc, obtain $L \propto T^2$ independent of mass, if radiative cooling is not implemented. In contrast, Bryan & Norman (1998), using simulations with 512^3

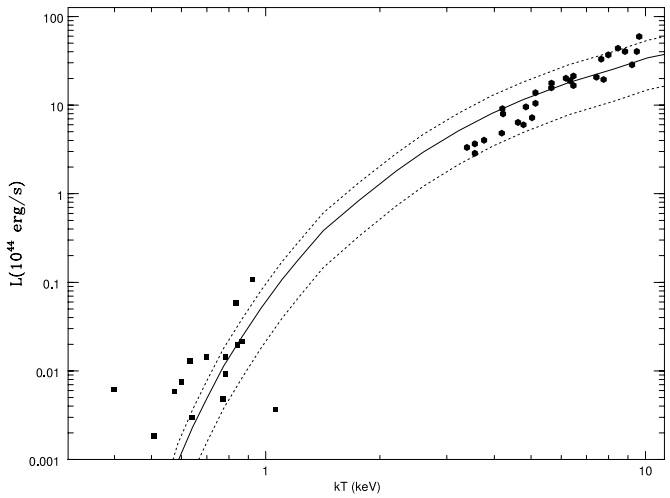

FIG. 2.—MPEM model. Shown is the average *L-T* correlation with a 2 σ dispersion (*dotted lines*), for a tilted cosmogony. Group data from Ponman et al. (1999) are represented by filled squares, while cluster data from Markevitch (1998) are represented by filled hexagons.

[10] One interesting point to mention, at this point, is that several different assumptions are able to reproduce the observed *L-T* relation. This could mean that *L-T* is not a very sensitive test since almost any change to the "pure" self-similar model reproduces this relation.

particles and a spatial resolution of 50 h^{-1} Mpc, did reproduce the observational bend of the L-T relation at the low-mass region.

A priori, it is unclear why the L-T and M-T relations are that sensitive to resolution. One possible explanation goes in the direction of the results shown in this paper. Taking into account that protostructures gain angular momentum owing to tidal interactions with other nonspherical structures, low resolution may hinder the gain of angular momentum by preventing an accurate determination of the protostructure shape. To clarify this point, we shall use the simulations of Muanwong et al. (2001) and Bryan & Norman (1998) as an example. The particle mass m_p of the first was $m_p = 2.1 \times 10^{10}\ h^{-1}\ M_\odot$, whereas the later used $m_p \simeq 6 \times 10^8\ h^{-1}\ M_\odot$ in their simulations. Since a common characteristic of hydrodynamic calculations is that all particles have the same mass, clusters with $kT < 2$ keV (where the bend in the L-T relation starts to depart clearly from self-similarity) have masses of $M \sim 3 \times 10^{14}\ h^{-1}\ M_\odot$; i.e., they contain approximately $N < 1.4 \times 10^4$ and $N < 5 \times 10^5$ particles in the Muanwong et al. (2001) and Bryan & Norman (1998) simulations, respectively. As we go to lower masses, we reduce the number of particles enclosed in protostructures. As a consequence, the shape and therefore the inertia axes may fluctuate randomly, which would lead on average to a systematic decrease of angular momentum gained by low-mass protoclusters.

Besides the poorly determined shape of low-mass structures, one must also take into account the possible effects of force resolution. In a typical N-body evolution code, such as TREECODE in Hernquist (1987), for example, the force acting on a particle is given by the sum of two components: the force coming from the nearest neighbors and that coming from an expansion of the gravitational potential of the entire system up to quadrupole terms. As can be shown, the value of the average stochastic force in the simulation, $F_{\rm sim}$, is an order of magnitude greater than that obtained from the theory, $F_{\rm th}$, of stochastic forces. As a consequence only the higher force are taken into account, while the small fluctuations induced by the small-scale substructure are not "seen." This is the case for CDM models in which the stochastic force generators are substructures at least three orders of magnitude smaller in size than the protostructures in which they are embedded (e.g., clusters of galaxies).

Taking into account the large simulations required to obtain a good description of the L-T relation, it is not surprising that similar disagreements are reported in other cases too. For example, in the case of the M-T relation, it is noted that the results from different observational methods of mass measurements are not consistent with one another and with the simulation results (e.g., Horner et al. 1999; Neumann & Arnaud 1999; Nevalainen et al. 2000; Finoguenov et al. 2001). In general, X-ray mass estimates are about 80% lower than the predictions of hydrosimulations. On the other hand, X-ray mass estimates lead to normalizations about 50% higher than our result and simulations.

One possible source of difference between theoretical and observational normalizations is that the values for $\tilde{\beta}$[11] are different in the two cases due to systematic selection effects. Also, intriguingly, Bryan & Norman (1998) showed that there is a systematic increase in the obtained value of $\tilde{\beta}$ by increasing the resolution of the simulations.

We would like to stress that even if the effects of angular momentum are not taken into account, this last process gives rise to self-similar structures only in a first approximation. In fact, (1) the effective spectral index $n_{\rm eff}$ of CDM models depends, even if weakly, on the scale, going from values of $n_{\rm eff} \simeq -1.2$ for clusters to $n_{\rm eff} \simeq -2$ for galaxies; (2) we live in a universe with a cosmological constant different from zero, which means that there is a typical redshift at which it became important for cosmic dynamics; (3) even DM profiles are not perfectly self-similar, since they depend on the concentration parameter, which in turn is inversely proportional to mass because smaller structures formed, on average, at earlier times, when cosmic density was larger.

As reported, Figure 1 shows a slight difference between the SMMS prediction and that of PEM, with the slope predicted by SMSS at low temperatures being less steep than that of PEM and MPEM. The difference is not large, implying a difference in luminosity of 10% (larger for SMSS with respect to PEM). Also plotted in Figure 1 is the L-T relation predicted by MPEM. In this last case, the bending is produced by two effects: the threshold effect of the preheating temperature $kT_1 \simeq 0.5$ keV (as in CMT99) and the effect of angular momentum acquired by clusters. As a consequence, if we compare MPEM with PEM (or MSSM), the bending is larger (besides the threshold effect, we have the acquisition of angular momentum).

Relative to this last item, looking at Figure 1 one can see that the curve obtained from MSSM is very different from that corresponding to SSM, whereas the one from MPEM differs not much from that of PEM. The reason is the following: if we consider a cluster, without implementing preheating, the angular momentum acquisition is responsible for the slowing down and eventual stopping of the matter collapse toward the center of the cluster, leading to the consequences we have discussed. Implementing preheating, this gives rise (by heating the uncondensed gas and therefore making it harder to compress in the core) to a region at higher temperature and pressure that acts like a boundary for the infalling gas, which therefore reduces the effects induced by angular momentum acquisition.

In Figure 2 we plot the results for the MPEM model: the average L-T correlation with the 2 σ dispersion (*dotted lines*) for a tilted cosmogony. Group data from Ponman et al. (1999) are represented by filled squares, while cluster data from Markevitch (1998) are represented by filled hexagons. The L-T correlation is given by the double convolution (eq. [10]), while ΔL is obtained by equation (11). The normalization has been fitted to the data (see CMT99).

The quantities and profiles of the PEM model are the same as those of CMT99, namely, the reference cluster has a mass $m = M/M_0$ and a DM potential $\phi(r)$, as described in Appendix B. The density and temperature profiles are given by equation (30), and they should match the shock boundary conditions at the position $r_2 \simeq R_{\rm vir}$. The average value and scatter of the parameter β given by equation (31), calculated through the PEM and shown in Figure 2 of CMT99, increases from $\beta = 0.5$ to $\beta \simeq 0.9$, while the baryonic fraction f_2 is the one in Figure 3 of CMT99. The γ-parameter is fixed as described in Appendix B. As the plot shows, in agreement with CMT99, the correlation is not a simple power law but starts as $L \propto T^2$ for very rich clusters, and then it bends down with decreasing T. As previously noted, the bending is induced by two mechanisms: the threshold imposed by the preheating temperature $kT_1 \simeq 0.5$ keV (as in CMT99) and the angular momentum acquired by clusters. As a consequence, if we compare MSSM with PEM, the bending is larger (beside the threshold effect we have the acquisition of angular momentum).

We want to point out a similarity between the role of preheating temperature T in the PEM and that of the angular momentum $\mathcal{L}$ in our model. In the PEM, the thermal energy of infalling gas comes initially from stellar preheating (of nuclear origin); then it is increased to the virial value (of gravitational origin) when the

[11] $\tilde{\beta} = \beta[1 + f(1/\beta - 1)\Omega_b/\Omega_m]$, where f is the fraction of the baryonic matter in the hot gas, and Ω_b is the density parameter of the baryonic matter.

accreted gas is bound to DM subclumps. So the preheating sets an effective threshold $kT_1 \sim 0.5$ keV to gas inclusion, which breaks the self-similar correlation $L \propto T^2$ not only in its vicinity but also up to a few keV. Increasing the preheating temperature, the bending in the L-T relation becomes more pronounced. A similar process occurs if the acquired angular momentum is larger.

A fitting formula similar to that of CMT98 for the predicted L-T correlation (for $T > T_1 \simeq 1$ keV) is given by

$$L = a_L T^{2+\alpha_L} (\rho/\rho_o)^{1/2},$$
$$a_L \propto \Omega_0^{0.3}(1+z)^{0.22/\Omega_0} + (1-\Omega_0)e^{-0.7(1+z)},$$
$$\alpha_L = a_1(1+z)^{-0.2} e^{-a_2(T-T_1)/\Omega_0^{0.1}(1+z)^{0.5}}, \qquad (12)$$

where the luminosity is expressed in units of 10^{44} ergs s^{-1} and the temperature in keV, and with $a_1 = 1.2$ and $a_2 = 0.17$.

At temperatures larger than the threshold $kT_1 \simeq 0.5$ keV, the relative $\Delta L/L$ remains constant around 25%. A study of the dependence of $\langle L \rangle$ and ΔL on Ω_0 shows that both these quantities increase with increasing Ω_0, similarly to what shown in CMT99.[12]

Figure 3 shows MSSM compared with observational data. Similarly to Figure 2, we plot the average L-T correlation with the 2 σ dispersion (*dotted lines*) for a tilted cosmogony. Group data from Ponman et al. (1999) are represented by filled squares, while cluster data from Markevitch (1998) are represented by filled hexagons. The L-T correlation can be fitted in this case by a formula similar to that of equation (13), with $a_1 = 1.28$ and $a_2 = 0.19$. As reported, Figure 1 shows a slight difference between the SMMS prediction and that of PEM, with the slope predicted by SMSS at low temperatures being less steep than that of PEM. The difference is not large, implying a difference in luminosity of 10% (larger for SMSS). The fit of the SMSS model to the data, as Figure 3 shows, is also very good.

To summarize, the key idea of the SMSS model and of other mechanisms proposed to reproduce the non–self-similarity of the L-T relation is in all cases fairly similar: if one wants to have clusters less luminous than the SSM prediction, it is necessary to have a physical process that reduces the quantity of gas infalling toward the center of the cluster, which therefore reduces the core luminosity. In the case of heating/cooling models, some energy input preheats the gas before it falls into new groups and clusters, hindering its flow into the latter. In the SMSS model, that role is played by the initial spin present in protoclusters.

[12] This is because the underlying strength of the current shocks grows on average as the merging rate (moderately) increases on approaching the critical cosmology; see Lacey & Cole (1993).

4. CONCLUSIONS

In this paper we have shown that the presence of angular momentum during the collapse of a protostructure leads to a non–self-similar L-T relation. The quoted effect leads, in X-rays, to a luminosity-temperature relation that scales as $L \propto T^5$ at the scale of groups, flattening to $L \propto T^3$ for rich clusters and converging to $L \propto T^2$ at higher temperatures.

These results are in disagreement with the largely accepted assumption that heating/cooling and similar processes are fundamental in originating the non–self-similar behavior (shaping) of the L-T relation. As Bryan & Norman (1998) showed, it is not necessary to hypothesize preheating/cooling models in order to reproduce observations; on the contrary, it is possible to reproduce the observed L-T relation if the spatial and mass resolution are accurate enough. Poorly resolved clusters, with few particles enclosed, lead to self-similar L-T curves.

We have shown that the large bend of the L-T relation is caused by the fact that the angular momentum acquired by a shell centered on a peak in the CDM density distribution is anticorrelated with density: high-density peaks acquire less angular momentum than low-density peaks. A greater amount of angular momentum acquired by low-density peaks (with respect to the high-density ones) implies that these peaks can more easily resist gravitational collapse and consequently that it is more difficult for them to form structure. This results in a tendency for less dense regions to accrete less mass with respect to a classical spherical model. As a consequence, the X-ray luminosities of low-temperature clusters are small because their gas is less centrally concentrated than in hotter clusters.

N. Hiotelis acknowledges the Empirikion Foundation for its financial support.

APPENDIX A

M-T RELATION

As previously noted, numerical methods and simple scaling arguments suggest that the X-ray temperature of clusters, T_X, can be directly related to their masses as $M_{vir} \propto T_X^{3/2} \rho_b^{-1/2} \Delta_{vir}^{-1/2}$, where ρ_b is the critical density and Δ_{vir} is the mean density within the virial radius R_{vir}.

In Del Popolo & Gambera (1999) and Del Popolo (2002b), we got the M-T relation in two different ways: (1) modifying the top-hat model, and (2) modifying the Voit & Donahue (1998) model. In the first, we modified the top-hat model in order to take account of angular momentum acquisition by protostructures and used a modified version of the virial theorem in order to include a surface pressure term (V00; AC02). This correction is due to the fact that at the virial radius R_{vir} the density is nonzero and that this requires a surface pressure term to be included in the virial theorem (Carlberg et al. 1997) (the existence of this confining pressure is usually not accounted for in the top-hat collapse model). The derivation of the previous relation is fundamentally based on the approximation of cluster formation with the evolution of a spherical top-hat density perturbation (Peebles 1993) and on the additional assumption that each cluster observed at a redshift z has just reached the moment of virialization. This last assumption is currently known as the late-formation approximation, which is a good one in a critical $\Omega_0 = 1$ case because for this value of Ω, massive clusters develop rapidly at all redshifts and the moment of virialization is always close to that of observation. In other words, for $\Omega_0 = 1$ the accretion rate remains sufficiently high, and this implies that the clusters we actually observe attained their observed masses recently. In the $\Omega_0 < 1$ case, cluster formation is "shutting down" and it is necessary to take account of the differences between the moment of virialization and that of observation. The problem becomes worse going through $\Omega_0 \ll 1$: in fact, in the late-formation approximation M_{vir} rises steadily since $\rho_b \Delta_{vir}$ declines indefinitely, while we expect that the cluster formation is going to stop.[13]

[13] The result of the late-formation approximation is displayed in eqs. (18) and (19) of Del Popolo (2002b).

The late-formation approximation is a good one for many purposes, but a better one can be obtained in the low-Ω limit. As can be found in the literature, there are two ways of improving the quoted model. One is to define a formation redshift z_f at which a cluster virializes, and then the properties of observed clusters at z are obtained by integrating over the appropriate distribution of formation redshifts (Kitayama & Suto 1996; Viana & Liddle 1996). The second possibility is the one described by Voit & Donahue (1998) and V00. In this approach, the top-hat cluster formation model is substituted by a model of cluster formation from spherically symmetric perturbations with negative radial density gradients. The fact that clusters form gradually, and not instantaneously, is taken into account in the merging-halo formalism of Lacey & Cole (1993). In hierarchical models of structure formation, the growth of the largest clusters is quasi-continuous since these large objects are so rare that they almost never merge with another cluster of similar size (Lacey & Cole 1993). So, the Lacey & Cole (1993) approach extends the Press-Schechter formalism by considering how clusters grow via accretion of smaller virialized objects. Summarizing, in order to obtain the proper normalization and time evolution of the *M-T* relation, one has to account for (1) the continuous accretion of mass of clusters and (2) the nonzero density at $R_{\rm vir}$, requiring a change in the virial theorem by including a surface pressure term.

The *M-T* relation derived by means of a model of continuous accretion differs from the late-formation model in both normalization and time-dependent behavior.[14]

In order to obtain the *M-T* relation in this second approach, we assume, as shown by V00, that the mass grows as $M \propto \omega^{-3/(n+3)}$ (Lacey & Cole 1993; Voit & Donahue 1998; V00).

In order to obtain an expression for the kinetic energy, we first calculated E/M:

$$\frac{E}{M} = -\frac{\int \epsilon\, dM}{M} = \frac{3m_1}{10(m_1-1)}\left(\frac{2\pi G}{t_\Omega}\right)^{2/3} M^{2/3}\left[\frac{1}{m} + \left(\frac{t_\Omega}{t}\right)^{2/3} + \frac{K_1(m_1,x)}{M^{8/3}}1\right], \tag{13}$$

$$K_1(m_1,x) = (m_1-1)Fx\,\mathrm{LerchPhi}\left(x,\ 1,\ \frac{3m_1}{5+1}\right) - (m_1-1)F\,\mathrm{LerchPhi}\left(x,\ 1,\ \frac{3m_1}{5}\right), \tag{14}$$

where

$$F = \frac{2^{7/3}\pi^{2/3}\xi\rho_{\rm b}^{2/3}}{3^{2/3}H^2\Omega}\int_0^r \frac{\mathcal{L}^2 dr}{r^3}, \tag{15}$$

$m_1 = 5/(n+3)$, $t_\Omega = \pi\Omega_0/H_0(1-\Omega_0-\Omega_\Lambda)^{3/2}$, $x = 1+(t_\Omega/t)^{2/3}$, which is connected to mass by $M = M_0 x^{-3m_1/5}$ (V00), and $\xi = r_{\rm ta}/x_1$, where $r_{\rm ta}$ is the turnaround radius and x_1 is defined by the relation $M = 4\pi\rho_b x_1^3/3$, where ρ_b is the background density. The LerchPhi function is defined as follows:

$$\mathrm{LerchPhi}\,(z,a,v) = \sum_{n=0}^{\infty}\frac{z^n}{(v+n)^a}. \tag{16}$$

The angular momentum $\mathcal{L}$ acquired by the protostructure is calculated using the same model (and same spectrum) as described in Del Popolo & Gambera (1998, 1999). More hints on the model and some of the model limits can be found in Del Popolo et al. (2001). Then the virial theorem with the surface pressure term correction, as in V00, is used in order to get a connection between the kinetic energy and temperature. We utilize the usual relation

$$\langle K\rangle = \frac{3\tilde{\beta}MkT}{2\mu m_p} \tag{17}$$

(AC02), where k is Boltzmann's constant, $\mu = 0.59$ is the mean molecular weight, m_p is the proton mass, and $\tilde{\beta} = \sigma_v^2/\left(kT/\mu m_p\right)$, where σ_v is the mass-weighted mean velocity dispersion of DM particles and $\tilde{\beta} = \beta[1+f(1/\beta-1)\Omega_b/\Omega_m]$, where f is the fraction of the baryonic matter in the hot gas and Ω_b is the density parameter of the baryonic matter. In this way, we finally get

$$kT = \frac{2}{5}a\frac{\mu m_p}{2\beta}\frac{m_1}{m_1-1}\left(\frac{2\pi G}{t_\Omega}\right)^{2/3} M^{2/3}\left[\frac{1}{m_1} + \left(\frac{t_\Omega}{t}\right)^{2/3} + \frac{K_1(m_1,x)}{M_0^{8/3}}\right], \tag{18}$$

where $a = \bar{\rho}/[2\rho(R_{\rm vir}) - \bar{\rho}]$ is the ratio between kinetic and total energy (V00). If $K_1 = 0$, equation (13) reduces to equation (10) of V00. As stressed by V00, some factors give rise to a higher value of E/M with respect the case of the late-formation value. The $m_1/(m_1-1)$ value accounts for the effect of early infall. The $1/m_1$ value in the square brackets of equation (13) accounts for the cessation of cluster formation when $t \gg t_\Omega$. Finally in equation (13) a new term is present, which comes from the tidal interaction.

[14] A comparison of the normalization predicted by the late-formation model with that predicted by simulations of Evrard et al. (1996) shows that when $\Omega_0 = 1$ this normalization is only 4% below the empirical value, but it lies 20% below it for $\Omega_0 = 0.2$. In the case of the V00 model and for a power-law spectrum, a comparison with the same simulations show that the temperature normalization of the $n = -2$ case deviates by less than 10% over the range $0.2 < \Omega_0 < 1$ and by $\simeq$18% in the case $n = -1$ (V00). The normalization obtained by the V00 model, even if it is more accurate than that given by late formation or by AC02, which is in agreement with hydro-simulations, shows a noteworthy discrepancy when compared with X-ray mass estimates (about 50% for the AC02 model; see also V00). One possible source of differences in theoretical and observational normalizations may be due to the fact that β is different in the two cases because of systematic selection effects. For example, as shown by Bryan & Norman (1998), increasing the resolution of simulations there is an increase in the value of β. So summarizing, concerning normalization the continuous-formation model gives more precise results than the late-formation one, but in any case if we want to fit observations we need to shift the normalization (see AC02).

Using the relation $\Delta_{\rm vir} = 8\pi^2/Ht^2$ (see V00) within the early-time limit ($t \ll t_\Omega$), equation (18) reduces to

$$kT = \frac{2}{5}\frac{m_1}{m_1 - 1} a \frac{\mu m_p}{2\beta} GM^{2/3} \left(\frac{4\pi}{3}\rho_b \Delta_{\rm vir}\right)^{1/3}, \tag{19}$$

which, in the case $n \sim -2$, $a \sim 2$, is identical to the late-formation formula described in V00 (see their eq. [8]). Normalizing equation (18) similarly to V00, we get

$$kT \simeq 8 \text{ keV} \left(\frac{M^{2/3}}{10^{15}\ h^{-1}\ M_\odot}\right) \left[\frac{1}{m_1} + \left(\frac{t_\Omega}{t}\right)^{2/3} + \frac{K_1(m_1, x)}{M^{8/3}}\right] \left[\frac{1}{m_1} + \left(\frac{t_\Omega}{t_0}\right)^{2/3} + \frac{K_0(m_1, x)}{M_0^{8/3}}\right]^{-1}, \tag{20}$$

where $K_0(m_1, x)$ indicates that $K_1(m_1, x)$ must be calculated assuming $t = t_0$

Equation (20), when compared to the result of V00 (their eq. [17]), shows an additional, mass-dependent term. This means that as in the case of the top-hat model, the *M-T* relation is no longer self-similar, showing a break at the low-mass end (see Appendix B).

APPENDIX B

L-T RELATION IN THE MODIFIED PUNCTUATED EQUILIBRIUM MODEL

The X-ray bolometric luminosity of a cluster is given by equation (1), which in CMT98's notation is

$$L \propto \int_0^{r_2} n^2(r) T^{1/2}(r) d^3 r. \tag{21}$$

Here $T(r)$ is temperature in the plasma and r_2 is the cluster boundary, which we take to be close to the virial radius $R_{\rm vir} \propto M^{1/3}\rho^{-1/3}$, where $\rho(z) \propto (1+z)^3$ is the DM density in the cluster, proportional to the average cosmic DM density $\rho_u(z)$ at formation. The infalling gas is expected to become supersonic near r_2 (see, e.g., Perrenod 1980; Takizawa & Mineshige 1998), so that a shock front will form there. The conservations across the shock of mass, energy, and stresses yield the Rankine-Hugoniot conditions, i.e., the temperature and density jumps from the outer values T_1 and n_1 to T_2 and n_2 just interior to r_2. Thus the luminosity can be rewritten in the form

$$L \propto r_2^3 n_2^2 T_2^{1/2} \int_0^1 d^3 x \left[\frac{n(x)}{n_2}\right]^2 \left[\frac{T(x)}{T_2}\right]^{1/2}, \tag{22}$$

where $x \equiv r/r_2$; n_1 is fixed by $n_1 \propto f_u \rho_u / m_p$ in terms of the universal baryonic fraction f_u, whereas T_1 is determined only statistically through the diverse merging histories ending up with the mass M. In sum, a given dark mass M admits a set of ICP equilibrium states characterized by different boundary conditions, each corresponding to a different realization of the dynamical merging history. It is the convolution over such a set that provides the average values of L and $R_{\rm X}$ and their scatter. Following CMT98, the preshock temperature in a merging event is that of the infalling gas, and if the latter is contained in a sufficiently deep potential well, T_1 is the virial temperature $T_{1v} \propto \Delta m / r$ of the secondary merging partner; on using $r \propto (\Delta m/\rho)^{1/3}$, this gives

$$kT_{1v} = 4.5 (\Delta m)^{2/3} (\rho/\rho_0)^{1/3} \text{ keV}, \tag{23}$$

where the numerical coefficient is taken from Hjorth et al. (1998) and the masses $m = M/M_0$ are normalized to the current value $M_0 = 0.6 \times 10^{15} \Omega_0\ h^{-1}\ M_\odot$ (i.e., the mass enclosed within a sphere of 8 h^{-1} Mpc), so in the following the actual value of T_1 is[15]

$$T_1 = \max(T_{1v},\ T_{1*}). \tag{24}$$

Given T_1, the boundary conditions for the ICP in the cluster are set by the strength of the shocks separating the inner from the infalling gas. In the case of three degrees of freedom and for a nearly hydrostatic postshock condition with $v_2 \ll v_1$, assuming that the shock velocity matches the growth rate of the virial radius $R_{\rm vir}(t)$,

$$kT_2 = \frac{\mu m_p v_1^2}{3} \left[\frac{\left(1 + \sqrt{1+\epsilon}\right)^2}{4} + \frac{7}{10}\epsilon - \frac{3}{20}\frac{\epsilon^2}{\left(1 + \sqrt{1+\epsilon}\right)^2}\right] \tag{25}$$

(CMT97).

Here $\epsilon \equiv 15 kT_1 / 4\mu m_p v_1^2$, and μ is the average molecular weight; the inflow velocity v_1 is set by the potential drop across the region of nearly free fall, to read $v_1 \simeq \left(-\phi_2/m_p\right)^{1/2}$ in terms of the potential ϕ_2 at r_2. In the case of strong shocks appropriate to "cold inflow" ($\epsilon \ll 1$), as in rich clusters accreting small clumps and diffuse gas, the approximation

$$kT_2 \simeq -\phi_2/3 + 3kT_1/2 \tag{26}$$

[15] An independent lower bound $kT_{1*} \approx 0.5$ keV is provided by preheating of diffuse external gas, due to feedback energy input following star formation and evolution all the way to supernovae (David et al. 1995; Renzini 1997).

holds, where ϕ_2 is the gravitational potential energy at $r_2 \simeq R_{\rm vir}$. For $\epsilon \geq 1$ the shock is weak and $T_2 \simeq T_1$. From T_2 and T_1, the density jump at the boundary n_2/n_1 is found to be (see CMT97)

$$\frac{n_2}{n_1} = 2\left(1 - \frac{T_1}{T_2}\right) + \left[4\left(1 - \frac{T_1}{T_2}\right)^2 + \frac{T_1}{T_2}\right]^{1/2}. \tag{27}$$

Adopting the polytropic temperature description $T(x)/T_2 = [n(x)/n_2]^{\gamma-1}$, with the index γ in the range $1 \leq \gamma \leq 5/3$, and given that the radius r_2 can be written in terms of temperature $T_v \propto m/r_2$ and that $m \propto \rho r_2^3$, leading to $r_2 \propto (t/\rho)^{1/2}$, the luminosity can be written in the form

$$L \propto \left(\frac{n_2}{n_1}\right)^2 m T_v^{1/2} \rho \left(\frac{T_2}{T_v}\right)^{1/2} \overline{[n(r)/n_2]^{2+(\gamma-1)/2}}, \tag{28}$$

where the bar denotes the integration over the emitting volume $r^3 \leq r_2^3$, and ρ is the average DM density in the cluster, proportional to ρ_u and so to n_1.

Equation (28) can be also cast in the form

$$L \propto \left(\frac{n_2}{n_1}\right)^2 \rho \left(\frac{T_2}{T_v}\right)^{1/2} \overline{[n(r)/n_2]^{2+(\gamma-1)/2}}\, m^{4/3} \sqrt{\frac{1/m_1 + (t_\Omega/t)^{2/3} + K/(m/m_0)^{8/3}}{1/m_1 + (t_\Omega/t)^{2/3} + K_0/m_0^{8/3}}}. \tag{29}$$

The ratio $n(x)/n_2$ is obtained from the hydrostatic equilibrium $dP/m_p n\, dr = -GM(<r)/r^2 = -d\phi/dr$ with the polytropic pressure $P(r) = kT_2 n_2 [n(r)/n_2]^\gamma$. This yields (see Cavaliere & Fusco-Femiano 1978; Sarazin 1988 and references therein) the profiles

$$\frac{n(r)}{n_2} = \left[\frac{T(r)}{T_2}\right]^{1/(\gamma-1)} = \left\{1 + \frac{\gamma - 1}{\gamma}\beta\left[\tilde{\phi}_2 - \tilde{\phi}(r)\right]\right\}^{1/(\gamma-1)}, \tag{30}$$

where $\tilde{\phi} \equiv \phi/\mu m_p \sigma_2^2$ is the potential normalized to the associated one-dimensional DM velocity dispersion at r_2. The ICP disposition in equation (11) relative to the DM depends on the previously encountered parameter

$$\beta = \mu m_p \sigma_2 / kT_2 \tag{31}$$

and is further modulated by the second parameter γ to yield, as the latter increases, flatter profiles $n(r)$ and steeper $T(r)$.[16]

The function $\beta(T)$ can be easily computed from equation (26) for a given DM potential ϕ_2 corresponding to $\rho(r)$; $\phi(r)$ and $\sigma(r)$ are obtained in agreement with Navarro et al. (1997).

APPENDIX C

CALCULATION OF THE ANGULAR MOMENTUM

The effect of tidal torques on structure evolution has been studied in several papers, especially in connection with the origin of galactic rotation (Hoyle 1949; Peebles 1969; White 1984; Ryden 1988, hereafter R88; Eisenstein & Loeb 1995).

Following Eisenstein & Loeb (1995), we separate the universe into two disjoint parts: the collapsing region, characterized by having high density, and the rest of the universe. The boundary between these two regions is taken to be a sphere centered on the origin. As usual, in the following we denote with $\rho(\boldsymbol{x})$, $\boldsymbol{x}$ being the position vector, the density as a function of space, and $\delta(\boldsymbol{x}) = [\rho(\boldsymbol{x}) - \rho_b]/\rho_b$. The gravitational force exerted on the spherical central region by the external universe can be calculated by expanding the potential $\Phi(\boldsymbol{x})$ in spherical harmonics. Assuming that the sphere has radius R, we have

$$\Phi(\boldsymbol{x}) = \sum_{l=0}^{\infty} \frac{4\pi}{2l+1} \sum_{m=-l}^{l} a_{lm}(x) Y_{lm}(\theta, \phi) x^l, \tag{32}$$

where Y_{lm} are spherical harmonics and the tidal moments a_{lm} are given by

$$a_{lm}(x) = \rho_b \int_R^\infty Y_{lm}(\theta, \phi) \rho(\boldsymbol{s}) s^{-l-1} d^3 s. \tag{33}$$

[16] For the King potential (see Sarazin 1988) and CMT97, with core radius $r_c = R_v/12$, $\beta(T)$ increases from $\beta \simeq 0.5$ for $T \simeq T_1$ to $\beta \simeq 0.9$ for $T \gg T_1$. A similar result is obtained for a Navarro et al. (1997) potential. The other parameter, γ, will be bounded according to CMT99; the polytropic index $\gamma \geq 1$ describes the equation of state for the ICP. An upper bound to it arises if the overall thermal energy of the ICP is not to exceed its gravitational energy. The thermal and the gravitational energy are computed using the profiles in eq. (30), and their ratio is given in Fig. 4 of CMT99, to show that the *upper* bound $\gamma \leq 1.3$ holds. It turns out that observations by Markevitch et al. (1998) are consistent with the $T(r)$ predicted when $\gamma = 1.2 \pm 0.1$, in our allowed range. Hereafter we focus on $\gamma = 1.2$.

In this approach the protostructure is divided into a series of mass shells and the torque on each mass shell is computed separately. The density profile of each protostructure is approximated by the superposition of a spherical profile $\delta(r)$ and a random CDM distribution $\varepsilon(\boldsymbol{r})$, which provides the quadrupole moment of the protostructure. To first order, the initial density can be represented by

$$\rho(\boldsymbol{r}) = \rho_b[1 + \delta(r)][1 + \varepsilon(\boldsymbol{r})], \tag{34}$$

where $\varepsilon(\boldsymbol{r})$ is given by

$$\left\langle |\varepsilon_k|^2 \right\rangle = P(k), \tag{35}$$

$P(k)$ being the power spectrum. The torque on a thin spherical shell of internal radius x is given by

$$\tau(x) = -\frac{GM_{\rm sh}}{4\pi} \int \varepsilon(\boldsymbol{x}) \boldsymbol{x} \times \nabla\Phi(\boldsymbol{x}) d\Omega, \tag{36}$$

where $M_{\rm sh} = 4\pi\rho_b[1 + \delta(x)]x^2\delta x$. Before going on, I want to recall that we are interested in the acquisition of angular momentum from the inner region, and for this purpose we take account only of the $l = 2$ (quadrupole) term. In fact, the $l = 0$ term produces no force, while the dipole ($l = 1$) cannot change the shape or induce any rotation of the inner region. As shown by Eisenstein & Loeb (1995), in the standard CDM scenario the dipole is generated at large scales, so the object that we are studying and its neighborhood move as a bulk flow, with the consequence that the angular distribution of matter will be very small and thus the dipole terms can be ignored. Because of the isotropy of the random field $\varepsilon(\boldsymbol{x})$, equation (36) can be written as

$$\left\langle |\tau|^2 \right\rangle = \sqrt{30}\frac{4\pi G}{5}\left[\left\langle a_{2m}(x)^2\right\rangle\left\langle q_{2m}(x)^2\right\rangle - \left\langle a_{2m}(x) q^*_{2m}(x)\right\rangle^2\right]^{1/2}, \tag{37}$$

where $\langle \cdots \rangle$ indicates a mean value of the physical quantity considered. As stressed below, following Eisenstein & Loeb (1995) the integration of the equations of motion will end at some time before the inner external tidal shell (i.e., the innermost shell of the part of the universe outside the sphere containing the ellipsoid) collapses. Then the inner region behaves as a density peak. This last point is an important one in the development of the present paper.

An important question to ask, before going on, regards the role of triaxiality of the ellipsoid (density peak) in generating a quadrupole moment. Equation (37) takes into account the quadrupole moment coming from the secondary perturbation near the peak. The density distribution around the inner region is characterized by a mean spherical distribution δ and a random isotropic field. In reality the central region is a triaxial ellipsoid. It is then important to evaluate the contribution to the quadrupole moment due to the triaxiality. We remember that the quadrupole moments are given by

$$q_{2m} = \int_{|\boldsymbol{r}|<R} Y^*_{2m}(\theta,\phi) s^2 \rho(\boldsymbol{s}) d^3 s = \frac{x^2 M_{\rm sh}}{4\pi} \int Y^*_{2m}(\theta,\phi)\varepsilon(\boldsymbol{x}) d\Omega \tag{38}$$

and approximate the density profile as

$$\delta(\boldsymbol{x}) = \langle\delta(x)\rangle_{\rm spherical} + \nu f(x) A(e,p), \tag{39}$$

where $\langle\delta(x)\rangle_{\rm spherical}$ is the mean spherical profile, $\nu = \delta/\sigma$ is the peak height, and σ is the rms value of δ. The function $A(e,p)$ of the triaxiality parameters e and p is given by

$$A(e,p) = 3e(1 - \sin^2\theta - \sin^2\theta\sin^2\phi) + p(1 - 3\sin^2\theta\cos^2\phi), \tag{40}$$

while the function $f(x)$ is given (R88) by

$$f(x) = \frac{5}{2\sigma} R_*^2 \left(\frac{1}{x}\frac{d\xi}{dx} - \frac{1}{3}\nabla^2\xi\right), \tag{41}$$

where ξ, σ, and R_* are respectively the two-point correlation function, the mass variance, and a parameter connected to the spectral moments (see Bardeen et al. 1986, hereafter B86, eq. [4.6d]). Substituting equations (39) and (40) into equation (38), it is easy to show that the sum of the mean quadrupole moments due to triaxiality is

$$\frac{1}{M_{\rm sh}}\sum_{m=-2}^{2}\langle q_{2m}(x)\rangle = \nu x^2 f(x)\left[\frac{1}{2\pi}\sqrt{\frac{6\pi}{5}}(e-p) + \frac{1}{4\pi}\sqrt{\frac{4\pi}{5}}(3e+p)\right], \tag{42}$$

which must be compared with that produced by the secondary perturbations ε:

$$\left\langle q_{2m}(x)^2\right\rangle = \frac{x^4}{(2\pi)^3} M_{\rm sh}^2 \int k^2 P(k) j_2(kx)^2 dk, \tag{43}$$

where j_2 is the Bessel function of order 2. The values of e and p can be obtained from the distribution of ellipticity and prolateness (B86, eq. [7.6] and Fig. 7) or for $\nu > 2$ by

$$e = \frac{1}{\sqrt{5}x[1 + 6/(5x^2)]^{1/2}} \tag{44}$$

and

$$p = \frac{6}{5x^4[1 + 6/(5x^2)]^2} \tag{45}$$

(B86, eq. [7.7]), where x is given in B86 (eq. [6.13]). In the case of a peak with $\nu = 3$, we have $e \simeq 0.15, p \simeq 0.014$, while for peaks having $\nu = 2$ and $\nu = 1$ these are respectively given by $e \simeq 0.2,\ p \simeq 0.03$ and $e \simeq 0.25,\ p \simeq 0.04$.

As shown in Figure 1 of Del Popolo et al. (2001), for a 3 σ profile the source of the quadrupole moment due to triaxiality is less important than that produced by the random perturbations ε in all of the protostructure, except in the central regions where the quadrupole moment due to triaxiality is comparable in magnitude to that due to secondary perturbations. In other words, the triaxiality has a significant effect only in the very central regions, which contain no more than a few percent of the total mass and where the acquisition of angular momentum is negligible. It follows that the triaxiality can be ignored while computing both expansion and spin growth (R88). Moreover, as observed by Eisentein & Loeb (1995) the ellipsoid model does better in describing low-shear regions (having higher values of ν), whose collapse is more spherical and thus for which the effects of triaxiality are less evident. Just the peaks having at least $\nu > 2$ are studied in this paper. In any case, even if the triaxiality is not negligible it should contribute to incrementing the acquisition of angular momentum (Eisenstein & Loeb 1995) and finally to a larger effect on the density evolution (i.e., a larger reduction of the growing rate of the density).

In order to find the total angular momentum imparted to a mass shell by tidal torques, it is necessary to know the time dependence of the torque. This can be done connecting q_{2m} and a_{2m} to parameters of the spherical collapse model (Eisenstein & Loeb 1995, eq. [32]; R88, eqs. [32] and [34]). Following R88 we have

$$q_{2m}(\theta) = \frac{1}{4} q_{2m,0} \bar{\delta}_0^{-3} \frac{(1 - \cos\theta)^2 f_2(\theta)}{f_1(\theta) - \left(\delta_0/\bar{\delta}_0\right) f_2(\theta)} \tag{46}$$

and

$$a_{2m}(\theta) = a_{2m,0} \left(\frac{4}{3}\right)^{4/3} \bar{\delta}_0 (\theta - \sin\theta)^{-4/3}. \tag{47}$$

The collapse parameter θ is given by

$$t(\theta) = \frac{3}{4} t_0 \bar{\delta}_0^{-3/2} (\theta - \sin\theta). \tag{48}$$

Equations (46) and (47), by means of equation (37), give to us the tidal torque:

$$\tau(\theta) = \tau_0 \frac{1}{3} \left(\frac{4}{3}\right)^{1/3} \bar{\delta}_0^{-1} \frac{(1 - \cos\theta)^2}{(\theta - \sin\theta)^{4/3}} \frac{f_2(\theta)}{f_1(\theta) - \left(\delta_0/\bar{\delta}_0\right) f_2(\theta)}, \tag{49}$$

where $f_1(\theta)$ and $f_2(\theta)$ are given in R88 (eq. [31]), and τ_0 and $\delta_0 = (\rho - \rho_b)/\rho_b$ are respectively the torque and the mean fractional density excess inside the shell, as measured at current epoch t_0. The angular momentum acquired during expansion can then be obtained by integrating the torque over time:

$$L = \int \tau(\theta) \frac{dt}{d\theta} d\theta. \tag{50}$$

As remarked in the Del Popolo et al. (2001), the angular momentum obtained from equation (50) is evaluated at the time of maximum expansion t_M. Then the calculation of the angular momentum can be solved by means of equation (50), once we have made a choose for the power spectrum. With the power spectrum and the parameters given above and for a $\nu = 2$ peak, the model gives a value of 2.5×10^{74} g cm^2 s^{-1}. As previously quoted, we assume that from t_M on, the ellipsoid has this constant angular momentum. Following procedures 1 and/or 2 given in Appendix A, we are able to get the time evolution of the density.

REFERENCES

Afshordi, N., & Cen, R. 2002, ApJ, 564, 669 (AC02)
Allen, S. W., & Fabian, A. 1998, MNRAS, 297, L57
Allen, S. W., Schmidt, R. W., & Fabian, A. C. 2001, MNRAS, 328, L37
Audit, E., Teyssier, R., & Alimi, J. M. 1997, A&A, 325, 439
Balogh, M. L., Babul, A., & Patton, D. R. 1999, MNRAS, 307, 463
Bardeen, J. M., Bond, J. R., Kaiser, N., & Szalay, A. S. 1986, ApJ, 304, 15 (B86)
Barnes, J., & Efstathiou, G. 1987, ApJ, 319, 575
Barrow, J. D., & Silk, J. 1981, ApJ, 250, 432
Bialek, J. J., Evrard, A. E., & Mohr J. J. 2001, ApJ, 555, 597

Bond J. R., & Myers, S. T. 1993a, in The Evolution of Galaxies and their Environment: Proc. Third Teton Summer School, ed. D. J. Hollenbach, H. A. Thronson, & J. M. Shull (NASA CP-3190; Moffett Field: NASA), 21
———. 1993b, in The Evolution of Galaxies and their Environment: Proc. Third Teton Summer School, ed. D. J. Hollenbach, H. A. Thronson, & J. M. Shull (NASA CP-3190; Moffett Field: NASA), 52
Borgani, S., et al. 2001, ApJ, 559, L71
Bower, R. G., Castander, F. J., Couch, W., Ellis, R. S., & Böhringer, H. 1997, MNRAS, 291, 353
Bryan, G. L. 2000, ApJ, 544, L1
Bryan, G. L., & Norman, M. L. 1998, ApJ, 495, 80
Carlberg, R. G., Yee, H. K. C., & Ellingson, E. 1997, ApJ, 478, 462
Catelan, P., & Theuns, T. 1996, MNRAS, 282, 436
Cavaliere, A., & Fusco-Femiano, R. 1978, A&A, 70, 677
Cavaliere, A., Menci, N., & Tozzi, P. 1997, ApJ, 484, L21 (CMT97)
———. 1998, ApJ, 501, 493 (CMT98)
———. 1999, MNRAS, 308, 599 (CMT99)
David, L. P., Jones, C., & Forman, W. 1995, ApJ, 445, 578
David, L. P., Slyz, A., Jones, C., Forman, W., & Vrtilek, S. D. 1993, ApJ, 412, 479
Davis, M., & Peebles, P. J. E. 1977, ApJS, 34, 425
Del Popolo, A. 2002a, A&A, 387, 759
———. 2002b, MNRAS, 336, 81
Del Popolo, A., Ercan, E. N., & Xia, Z. Q. 2001, AJ, 122, 487
Del Popolo, A., & Gambera, M. 1998, A&A, 337, 96
———. 1999, A&A, 344, 17
Edge, A. C., & Stewart, G. C. 1991, MNRAS, 252, 414
Efstathiou, G., & Jones, B. J. T. 1979, MNRAS, 186, 133
Eisenstein, D. J., & Loeb, A. 1995, ApJ, 439, 520
Eke, V. R., Cole, S., & Frenk, C. S. 1996, MNRAS, 282, 263
Evrard, A. E., & Henry, J. P. 1991, ApJ, 383, 95
Evrard, A. E., Metzler, C. A., & Navarro, J. F. 1996, ApJ, 469, 494
Finoguenov, A., Reiprich, T. H., & Böhringer, H. 2001, A&A, 368, 749
Gioia, I., Henry, J. P., Maccacaro, T., Morris, S. L., Stocke, J. T., & Wolter, A. 1990, ApJ, 356, L35
Henry, J. P., Gioia, I., Maccacaro, T., Morris, S. L., Stocke, J. T., & Wolter, A. 1992, ApJ, 386, 408
Hernquist, L. 1987, ApJS, 64, 715
Hiotelis, N. 2002, A&A, 382, 84
Hjorth, J., Oukbir, J., & van Kampen, E. 1998, MNRAS, 298, L1
Hoffman, Y. 1986, ApJ, 301, 65
Horner, D. J., Mushotzky, R. F., & Scharf, C. A. 1999, ApJ, 520, 78
Hoyle, F. 1949, in Problems of Cosmical Aerodynamics, ed. J. M. Burgers & H. C. van de Hulst (Dayton: Central Air Documents Office), 195
Kaiser, N. 1986, MNRAS, 222, 323
Kaiser, N. 1991, ApJ, 383, 104
Kitayama, T., & Suto, Y. 1996, ApJ, 469, 480
Kratsov, A. V., Klypin, A. A., Bullock, J. S., & Primack, J. R. 1998, ApJ, 502, 48
Lacey, C., & Cole, S. 1993, MNRAS, 262, 627
Lokas, E. L., Juskiewicz, R., Bouchet, F. R., & Hivon, E. 1996, ApJ, 467, 1
Markevitch, M. 1998, ApJ, 503, 77
Mathiesen, B. F. 2001, MNRAS, 326, L1
Muanwong, O., Thomas, P. A., Kay, S. T., Pearce, F. R., & Couchman, H. M. P. 2001, ApJ, 552, L27
Mushotzky, R. 1994, in Clusters of Galaxies, ed. F. Durret, A. Mazure, & J. Trân Thanh Vân (Gif-sur-Yvette: Editions Frontières), 167
Navarro, J. F., Frenk, C. S., & White, S. D. M. 1995, MNRAS, 275, 720
———. 1997, ApJ, 490, 493
Neumann, D. M., & Arnaud, M. 1999, A&A, 348, 711
Nevalainen, J., Markevitch, M., & Forman, W. 2000, ApJ, 532, 694
Peebles, P. J. E. 1969, ApJ, 155, 393
———. 1971, A&A, 11, 377
———. 1990, ApJ, 365, 27
———. 1993, Principles of Physical Cosmology (Princeton: Princeton Univ. Press)
Peebles, P. J. E., & Groth, E. J. 1976, A&A, 53, 131
Perrenod, S. C. 1980, ApJ, 236, 373
Ponman, T. J., Cannon, D. B., & Navarro, J. F. 1999, Nature, 397, 135
Renzini, A. 1997, ApJ, 488, 35
Ryden, B. S. 1988, ApJ, 329, 589 (R88)
Sarazin, C. L. 1988, X-Ray Emission from Clusters of Galaxies (Cambridge: Cambridge Univ. Press)
Shimizu, M., Kitayama, T., Sasaki, S., & Suto, Y. 2003, ApJ, 590, 197
Steinmetz, M., & Bartelmann, M. 1995, MNRAS, 272, 570
Szalay, A. S., & Silk, J. 1983, ApJ, 264, L31
Takizawa, M., & Mineshige, S. 1998, ApJ, 499, 82
Thomas, P. A., Muanwong, O., Kay, S. T., & Liddle, A. R. 2002, MNRAS, 330, L48
Tozzi, P., & Norman, C. 2001, ApJ, 546, 63
Viana, P. T. P., & Liddle, A. R. 1996, MNRAS, 281, 323
Villumsen, J. V., & Davis, M. 1986, ApJ, 308, 499
Voglis, N., & Hiotelis, N. 1989, A&A, 218, 1
Voit, G. M. 2000, ApJ, 543, 113 (V00)
Voit, G. M., & Bryan, G. 2001, Nature, 414, 425
Voit, G. M., & Donahue, M. 1998, ApJ, 500, L111
Warren, M. S., Quinn, P. J., Salmon, J. K., & Zurek, W. H. 1992, ApJ, 399, 405
White, R. E. 1991, ApJ, 367, 69
White, S. D. M. 1984, ApJ, 286, 38
Wu, K. K. S., Fabian, A. C., & Nulsen, P. E. J. 2000, MNRAS, 318, 889
Xu, H., Jing, G., & Wu, X. 2001, ApJ, 553, 78